

AD-A171 867

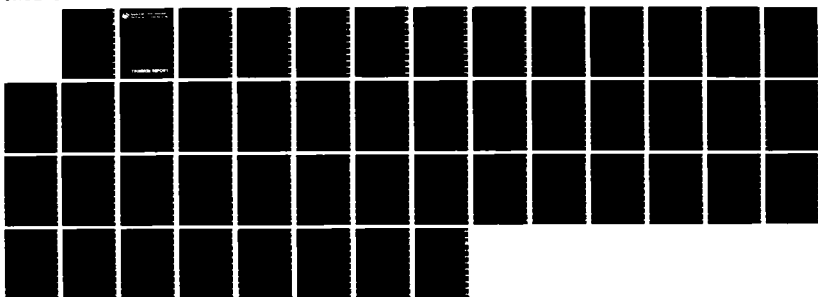
TWO DIMENSIONAL NON-LINEAR FINITE ELEMENT ANALYSIS OF
STRAIN ENERGY DENS. (U) PENNSYLVANIA STATE UNIV STATE
COLLEGE APPLIED RESEARCH LAB W L CROCKEN ET AL. JUN 86
TR-86-005

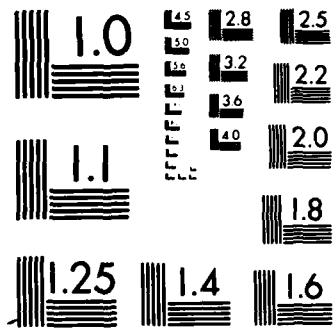
1/1

UNCLASSIFIED

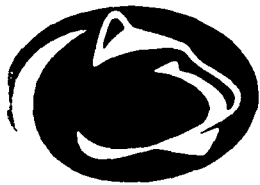
F/G 11/6

NL





1072



Applied Research Laboratory The Pennsylvania State University

AD-A171 867

12

TWO-DIMENSIONAL NON-LINEAR FINITE ELEMENT
ANALYSIS OF STRAIN ENERGY DENSITY
IN CRACKED A-517 STEEL PLATES

by

Michael L. Crocken and Ram B. Bhagat

SEP 17 1986
A

FILE COPY

This report has been approved
for release and its
contents are unlimited.



TECHNICAL REPORT

86 9 16 069

(2)

The Pennsylvania State University
Intercollege Research Programs and Facilities
APPLIED RESEARCH LABORATORY
P. O. Box 30
State College, Pennsylvania 16804

TWO-DIMENSIONAL NON-LINEAR FINITE ELEMENT
ANALYSIS OF STRAIN ENERGY DENSITY
IN CRACKED A-517 STEEL PLATES

by

Michael L. Crocken and Ram B. Bhagat

Technical Report 86-005
June 1986

SEP 17 1986
S
A

Supported by: Naval Sea Systems Command

L. R. Hettche, Director
Applied Research Laboratory

This document has been approved
for public release and sale; its
distribution is unlimited.

REPORT DOCUMENTATION PAGE

1a. REPORT SECURITY CLASSIFICATION		1b. RESTRICTIVE MARKINGS <i>AD-A171807</i>	
2a. SECURITY CLASSIFICATION AUTHORITY		3. DISTRIBUTION/AVAILABILITY OF REPORT Approved for public release; distribution unlimited	
2b. DECLASSIFICATION/DOWNGRADING SCHEDULE			
4. PERFORMING ORGANIZATION REPORT NUMBER(S)		5. MONITORING ORGANIZATION REPORT NUMBER(S)	
6a. NAME OF PERFORMING ORGANIZATION Applied Research Laboratory Penna. State University	6b. OFFICE SYMBOL (If applicable) ARL	7a. NAME OF MONITORING ORGANIZATION	
6c. ADDRESS (City, State, and ZIP Code) P. O. Box 30 State College, PA 16804		7b. ADDRESS (City, State, and ZIP Code)	
8a. NAME OF FUNDING/SPONSORING ORGANIZATION Naval Sea Systems Command	8b. OFFICE SYMBOL (If applicable) NAVSEA	9. PROCUREMENT INSTRUMENT IDENTIFICATION NUMBER	
8c. ADDRESS (City, State, and ZIP Code) Department of the Navy Washington, DC 20362		10. SOURCE OF FUNDING NUMBERS	
		PROGRAM ELEMENT NO.	PROJECT NO.
		TASK NO.	WORK UNIT ACCESSION NO.
11. TITLE (Include Security Classification) Two-Dimensional Non-Linear Finite Element Analysis of Strain Energy Density in Cracked A-517 Steel Plates			
12. PERSONAL AUTHOR(S) Michael L. Crocken and Ram B. Bhagat			
13a. TYPE OF REPORT B.S. Thesis	13b. TIME COVERED FROM _____ TO _____	14. DATE OF REPORT (Year, Month, Day) June 1996	15. PAGE COUNT 45
16. SUPPLEMENTARY NOTATION			
17. COSATI CODES		18. SUBJECT TERMS (Continue on reverse if necessary and identify by block number)	
FIELD	GROUP	two-dimension, non-linear, finite element analysis, strain energy density, steel, crack propagation, failure	
19. ABSTRACT (Continue on reverse if necessary and identify by block number)			
<p>A two-dimensional non-linear finite element analysis has been carried out to study the variation of the local strain energy density, $\frac{dW}{dV}$, in the neighborhood of a crack in A-517 steel compact tension specimens. It has been found that there exists a particular direction, θ_0, in which the variation of $\frac{dW}{dV}$ is anomalous to its well-known general decay from a very high value close to the crack tip to a low value farther away from the crack tip. This direction is considered as the probable</p>			
20. DISTRIBUTION/AVAILABILITY OF ABSTRACT <input type="checkbox"/> UNCLASSIFIED UNLIMITED <input type="checkbox"/> SAME AS RPT. <input type="checkbox"/> DTC USERS		21. ABSTRACT SECURITY CLASSIFICATION Unclassified	
22a. NAME OF RESPONSIBLE INDIVIDUAL		22b. TELEPHONE (include Area Code)	22c. OFFICE SYMBOL

(cont.)

direction of the crack propagation. This anomalous variation of the local strain energy density leads to the establishment of its two critical values, $(\frac{dIV}{dV})_{min}^*$ and $(\frac{dW}{dV})_{con}^*$, which are independent of the crack length and specimen geometry. It is suggested that the criticality of $(\frac{dIV}{dV})_{min}^*$ may signify a local instability ahead of the crack tip leading to the onset of crack initiation; in addition, the criticality of $(\frac{dW}{dV})_{con}^*$ may signify a global instability leading to the catastrophic fracture or plastic collapse of the specimen. It has also been demonstrated in the present study that the failure loads can be numerically and reliably predicted for any crack length.



Accession No.	
FILED	<input checked="" type="checkbox"/>
INDEXED	<input type="checkbox"/>
Classified	<input type="checkbox"/>
Justification	
By _____	
Distribution/	
Availability Codes	
and/or	
Dist. Special	
A-11	

TABLE OF CONTENTS

Table of Contents	iii
List of Figures	iv
List of Tables	v
I. INTRODUCTION	1
II. PROBLEM FORMULATION	12
III. SOFTWARE DEVELOPMENT	17
IV. FINITE ELEMENT MODELING	20
V. ANALYTICAL RESULTS AND DISCUSSION	24
VI. CONCLUSIONS	38
VII. REFERENCES	39

LIST OF FIGURES

<u>Figure</u>		<u>Page</u>
1	Graphical comparison of triangular and Quad-12 elements for a cantilever beam problem	11
2	Graphical depiction of the material modeling available in PAPST	16
3	The original model analyzed; Crack length = 1.537 inches	21
4	Experimental True Stress Strain curve for A-517 Steel used for bi-linear modeling	22
5	Global analysis of strain energy density versus radius (distance) from crack crack tip at a load of 4800 lb.	28
6	Comparison of strain energy density versus radius for nodes at 3 different angles from crack tip at a load of 4200 lb.	29
7	Comparison of strain energy density versus radius for different load increments at $\theta = 0^\circ$	30
8	Analysis of minimum strain energy density versus load at which that minimum occurs for a crack length of 1.537 inches	31
9	Shape of strain energy density versus radius curve at the critical load of 4980 lb.	32
10	Effects of crack length on minimum strain energy density versus radius curves	33
11	Strain energy density versus radius curves for specimen with crack length of 1.0 inches	34
12	Strain energy density versus radius curves for specimen with crack length of 1.643 inches	35
13	Effects of crack length on strain energy density versus radius curves	36
14	Effects of specimen width on strain energy density versus radius curves	37

LIST OF TABLES

<u>Table</u>		<u>Page</u>
1	Tabular comparison of triangular and Quad-12 elements for a cantilever beam problem	10
2	Compilation of different models analyzed in the present research	23

I. INTRODUCTION

Throughout history, the application of materials in engineering design has posed a variety of problems. In the nineteenth century, the industrial age ushered in a vast increase in the use of metals. It was soon discovered that structures made out of such materials were not perfect. Tragic accidents such as train wrecks and bridge collapses soon brought about widespread concern over the design of such structures. In many cases, the blame was correctly attributed to a poor basic design. Yet it was gradually discovered that metals had deficiencies in the form of pre-existing flaws, and such flaws could initiate cracks and fractures, thus bringing about failure of the structure.

The discovery of these flaws brought about an interest in studying metallic materials, for it was felt that prevention of such flaws would improve structural performance. Over the next several decades, the increase in the understanding of metallic behavior, combined with improved production methods, brought about a marked reduction in the number of structural failures.

In the second World War, a renewed interest in the study of materials came about as a result of the failure of several Liberty ships. Investigations into these failures revealed that flaws and stress concentrations were responsible for the brittle fractures. In the next several years, high strength materials were developed in the interest of weight savings. As many of these materials have low fracture toughness, it was discovered that they would fail at stresses below the service stress they were designed for in the presence of small cracks. This occurrence of low stress fracture in high strength materials has brought about the development of *fracture mechanics*. [1].

Although the majority of fracture mechanics has been developed in the last few decades, its beginnings can be traced back to the research of A.A.Griffith [2] in 1921. Griffith argued that in the case of uniaxial tensile loading of a material containing a crack perpendicular to the load, the crack would propagate and bring about catastrophic failure at a stress below its tensile strength. By analyzing the region surrounding the crack tip with respect to a global energy balance, Griffith developed the concept that a pre-existing crack can only extend catastrophically when the amount of elastic strain energy released on growth of the crack equals or exceeds the surface energy of the newly formed crack surfaces. The Griffith equation for the strength of a solid in plane stress containing a crack of length $2c$ was given as:

$$\sigma_f = \sqrt{\frac{2E\gamma}{\pi c}} \quad (1)$$

where E is Young's modulus, and γ is the surface energy [2-4].

Although Griffith's theory works well for purely brittle materials, it does not accurately describe the fracture situation in ductile materials. Griffith assumed that all of the work done during the fracture process goes into the creation of new surfaces; this does not allow for any dissipation of energy by plastic deformation and other energy dissipation mechanisms. As a result, the original Griffith criterion was extended by Irwin and Orowan [5,6] to include the case of ductile fracture of metals.

Irwin and Orowan noted that the energy required for a crack to extend in a metal is much greater than the surface energy of the new free surfaces. They proposed that a plastic work term γ_p should be added to the Griffith surface energy γ . Furthermore, they argued that γ_p is much greater than γ . Thus, γ_p replaced γ in Griffith's original equation, Eq. 1, as follows [5-7]:

$$\sigma_f = \sqrt{\frac{2E(\gamma + \gamma_p)}{\pi c}} \approx \sqrt{\frac{2E\gamma_p}{\pi c}} \quad (2)$$

Irwin later introduced the terms G and G_{Ic} for the plastic work associated with a spontaneously growing crack [3]. When G , the energy release rate or crack extension force, becomes equal to the critical value, G_{Ic} , the crack extension would then take place. This became known as the *critical energy release rate criterion* [1,7]. By substituting G_{Ic} for the surface energy term 2γ , Eq. 1 becomes:

$$\sigma_f = \sqrt{\frac{EG_{Ic}}{\pi c}} \quad (3)$$

The validity of Eq. 3 is limited to only linear elastic behavior of the specimen having a crack with practically no crack tip plasticity. However, if there exists a significant amount of plasticity, i.e., the crack tip plastic zone is large compared to the crack size, linear elastic fracture mechanics no longer applies. In 1961, A.A. Wells [8] introduced the critical crack opening displacement (COD) as a fracture criterion. This was originally developed as a criterion to treat those materials that exhibit a high ductility. Wells stated that crack extension is assumed to occur when the COD exceeds a critical value. One of the criterion's major drawbacks is the fact that it does not permit the direct calculation of a fracture stress [1,7]. The COD is found from:

$$COD = \frac{4(1 - \nu^2)K_{Ic}^2}{\pi E\sigma_{ys}} \quad (4)$$

where ν is Poisson's ratio, σ_{ys} is the yield strength, E is Young's modulus, and K_{Ic} is the mode I plane strain fracture toughness.

In 1968, J.R. Rice [9] introduced the application of a path-independent contour integral to analyze elastic-plastic crack problems. Similar in principle to the critical energy release rate criterion discussed above, Rice's *J-Integral* provides a fracture criterion for cases where plasticity effects are not negligible, and it is given as [7]

$$J = \int_{\Gamma} \left(W dy - (T_i \frac{\partial u_i}{\partial x}) ds \right) \quad (5)$$

$$\text{where } W = \int_0^{\epsilon_{ij}} \sigma_{ij} d\epsilon_{ij} \quad (6)$$

where the contour Γ is traversed in a counterclockwise direction from one crack face to the other, W is the strain energy density, T_i is the traction vector directed at a point on the contour Γ , u_i are the displacement components, and s is a measure of arc length along Γ . The crack is located in the xy - plane such that the crack lies parallel to the local x - axis.

The *J-Integral* has been widely used in non-linear fracture mechanics. It can be extended to critical values which will characterize the crack tip field at conditions of imminent fracture initiation. In the linear elastic case, the crack growth occurs if J exceeds a critical value J_{Ic} which is analogous to G_{Ic} . However, *J-Integral* is regarded as a more general criterion in that it is capable of handling both elastic and elastic-plastic fracture situations [1,10].

The independence of J on the contour path Γ chosen has been the subject of a great deal of research. Many results have indicated that J tends to decrease as the crack tip contour shrinks to the crack tip. In the elastic case of true path independency, however, J remains constant as the contour shrinks. In addition, J can be applied to only stationary cracks. Another limitation is that the plastic region around the crack tip must be small with respect to the size of the region in which J controls the stress field [1]. In the opinion of G.C.Sih, "There are too many fundamentally unresolved difficulties concerning the association of J with ductile fracture." [7]

At roughly the same time as Rice's *J-Integral* was introduced, another fracture criterion was developed using the crack resistance force R [7]. The criterion was based on comparing R to the energy release rate G . It was stated that:

- a) for $G < R$, no crack growth
- b) for $G = R$, stable crack growth
- c) for $G > R$, fracture instability occurs

An evaluation of this fracture criterion is possible upon analysis of the *R-curve*, a plot of G and R versus the crack length. At this stage, however, the theory for the *R-curve* has not been firmly established [1].

In 1973, G.C. Sih developed a new criterion based on the strain energy in the material, and termed it the *Strain Energy Density Criterion* [11,12]. The strain energy density in a solid can be calculated from either the area under the true stress-true strain diagram, or from [13]:

$$\frac{dW}{dV} = \frac{1}{2E} \left[\sigma_x^2 + \sigma_y^2 + \sigma_z^2 - 2\nu(\sigma_x\sigma_y + \sigma_y\sigma_z + \sigma_x\sigma_z) \right] + \frac{\tau_{xy}^2}{2G} \quad (7)$$

where σ_x , σ_y , σ_z are the normal stresses, τ_{xy} is the normal shearing stress, E is Young's Modulus, G is the shear modulus, and ν is Poisson's ratio. From this expression, Sih's *strain energy density factor* S can be analytically derived, and is given as:

$$S = r \left(\frac{dW}{dV} \right) \quad (8)$$

The *Strain Energy Density Criterion* is given in two parts:

- a. Crack initiation takes place in a direction θ_0 determined by the relative minimum of the strain energy density factor S :

$$S \rightarrow S_{min} \quad \text{at} \quad \theta = \theta_0 \quad (9)$$

- b. Rapid crack growth occurs when the minimum strain energy density factor S_{min} reaches a critical value:

$$S_{min} \rightarrow S_c \quad (10)$$

The general expression for S_c , the *critical strain energy density factor*, is derivable from experiments only, and is given as:

$$S_c = r_c \left(\frac{dW}{dV} \right)_c \quad (11)$$

where $\left(\frac{dW}{dV} \right)_c$ is the experimentally determined value of $\frac{dW}{dV}$ at fracture, and r_c is some critical radius of a core region surrounding the crack tip. Within the limits of linear elastic fracture mechanics, S_c can be related to the mode I plane strain fracture toughness K_{Ic} as follows:

$$S_c = \frac{(1 + \nu)(1 - 2\nu)}{2\pi E} K_{Ic}^2 \quad (12)$$

The ultimate goal in our research was to find a suitable fracture mechanics criterion that could be extended into a fracture mechanics theory for composite materials. In composites, it is most likely that a crack will not propagate in a self-similar manner. All fracture mechanics theories except that of Sih's assume directly or indirectly that the crack *must* propagate in a self-similar manner. This is the main reason why we were attracted to Sih's *Strain Energy Density Criterion* in our research.

The main criticism of Sih's criterion lies in the fact that although the definition of S is a purely analytical expression, the definition of S_c is not purely analytical. Although r can be substantiated analytically, r_c cannot be; furthermore, r_c has no physical significance. Likewise, although $\frac{dW}{dV}$ is well founded analytically, $\left(\frac{dW}{dV} \right)_c$ can be determined only from experimental true stress strain curves.

Finite element analysis was chosen as the tool through which our research was performed. One of the objectives in our research was to determine how the strain energy density $\frac{dW}{dV}$ behaves in the presence of a crack on a *local level*. This local $\frac{dW}{dV}$ is distinguished from a global $\frac{dW}{dV}$ in that the latter is determined from calculating the area under an experimental true stress-true strain diagram. Finite element analysis was chosen to conduct a local energy analysis, as it is obviously impossible to conduct such an analysis experimentally.

Acceptance for employing the finite element method in non-linear situations is dependent on several factors. To begin with, considerable computing power is required to solve problems with this degree of complexity. Yet improvements in digital computers over the last decade of so have increased computing power while lowering the computing costs. Secondly, the accuracy of any proposed solution technique must be proven before non-linear finite element analysis can be applied to design.

In the present study, an elastic-plastic stress analysis was performed on A-517 steel plates in order to observe the local behavior of the strain energy density in the vicinity of the crack. A-517 is a low carbon, quenched and tempered alloy steel intended primarily for use in welded bridges and other structures. Compared to other high-strength steels, A-517 exhibits a very high yield strength as well as good low temperature toughness [14,15].

Thus, the objectives of the present investigation were as follows:

1. Develop a suitable finite element analysis program to perform a non-linear stress analysis of cracked solids.
2. Use this finite element program to study local $\frac{dW}{dV}$ in cracked A-517 steel plates.

The finite element method is a numerical analysis technique utilized for obtaining solutions to an extensive variety of engineering problems. Any continuous quantity, such as stress, strain, pressure, or temperature, can be approximated by models constructed of a set of piecewise continuous functions defined over a finite number of elements. Using the concept that any continuous function can be represented by linear combinations of algebraic polynomials, approximation functions are derived for each of these elements. Elements are connected at common nodal points and collectively approximate the shape of the domain. The assemblage of elements is based on the concept that the solution is continuous at the boundaries

common to the elements [16-20].

There are generally six steps followed by the computer in the finite element method:

1. Read in input data (including the idealization)
2. Select interpolation or approximation function
3. Compute the properties desired for each element
4. Assemble the element properties
5. Obtain the system of equations
6. Solve the system of equations

The first step in preparing the input data is setting up an idealization to represent the structure (or, more generally, the domain). The resulting solutions for the program will obviously depend on the idealization created; it is here where experience in using finite element analysis is evidenced. Once certain guidelines are established, however, even a beginner can develop effective idealizations. These guidelines are as follows: [21]

1. Lay out the structure to scale, preferably on linear graph paper
 - a. If the structure is symmetrical, situate the structure so that one of the coordinate axes corresponds to the axis of symmetry.
 - b. Use enlargements or blowup areas where necessary
2. Divide the structure into a suitable number of elements; concentrate the elements in areas of high stress
3. Sketch in intermediate nodes along the element edges
4. Number the nodes using a suitable technique
5. Number the elements using a suitable technique
6. Compute nodal coordinates

A word on various types of elements is due at this point. The long-used constant-stress triangular element is now felt to be both obsolete, inefficient, and

surprisingly inaccurate [22]. This is readily evidenced upon comparison to today's *higher order elements* such as the 12-node isoparametric quadrilateral element (Quad-12 element). See Table 1 and Figure 1. The use of higher-order elements produces more accurate results in those areas where the gradient cannot be accurately approximated by sets of constant values. As opposed to the constant stress triangular elements, the Quad-12 element has a continuously varying stress field across its face. The displacement varies cubically within the Quad-12 element, as opposed to linearly in the constant-stress element. As a result, one Quad-12 element can replace as many as 200 triangular elements, thus reducing data preparation time and computer CPU time. In addition, the use of the Quad-12 element increases the accuracy of the solution.

The advantages of the Quad-12 element are thus:

1. Displacements vary cubically over the element. The element approximates the true displacement function with a third-degree polynomial degree fit.
2. The geometry of the element edges may vary cubically; thus, curved edges may be used to more closely approximate the structure.
3. As the stresses are given by appropriate first derivatives of the displacement functions, they vary quadratically over the element.

In numbering the nodes and elements, a technique is used in order to maximize the efficiency of the computer program. As a major part of the solution procedure in finite element analysis is the mathematical manipulation of matrices, the computation time is directly related to the size of these matrices. The set of equations that arise have a large number of coefficients which are zero. Upon analysis of a typical system matrix, it is seen that all non-zero coefficients will fall within two imaginary lines which can be constructed parallel to the main diagonal. The distance from the diagonal to this imaginary line is commonly referred to as the *bandwidth*. Reducing the bandwidth reduces the storage requirements for the program, thus reducing the

total computation time.

The most effective way to minimize the bandwidth is to number the nodes in the structural idealization in such a fashion as to keep the difference between numbers of adjacent nodes to a minimum. Similarly, the elements in the idealization should be numbered in the same fashion so as to minimize the difference between the numbers of adjacent elements [19,21]. The following section deals with the problem formulation.

Table 1. Tabular comparison of triangular and Quad-12 elements for a cantilever beam problem

Factor	Triangular	Quad-12
Number of Nodes	400	243
Number of Elements	686	3
Semibandwidth of Stiffness Matrix	20	24
Order of Stiffness Matrix	800	56
Required Computer Time on CDC 6400, sec.	53	6
Average Displacement Error, percent	-9	≈ 0
Average Stress Error, percent	-20	≈ 0
Manhours to prepare data	2	0.2
Turnaround Time	overnight	5 minutes

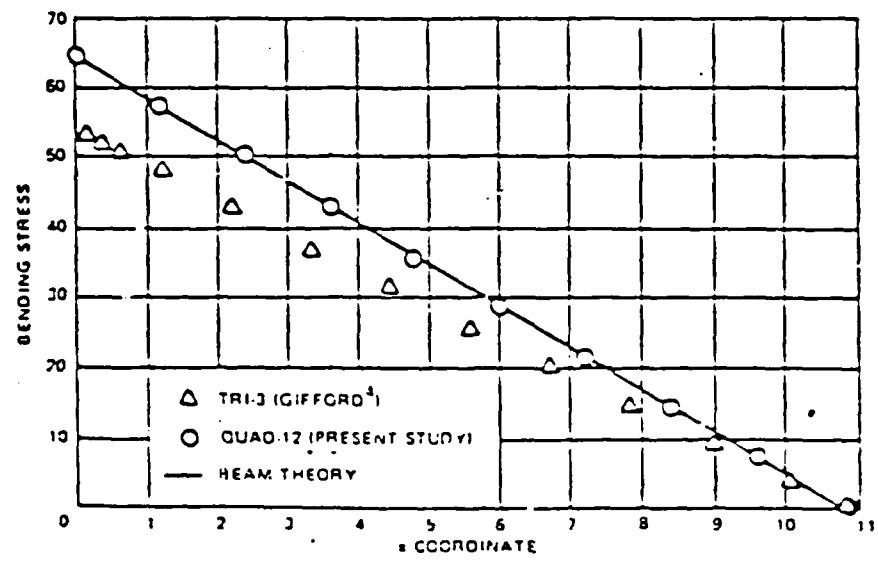
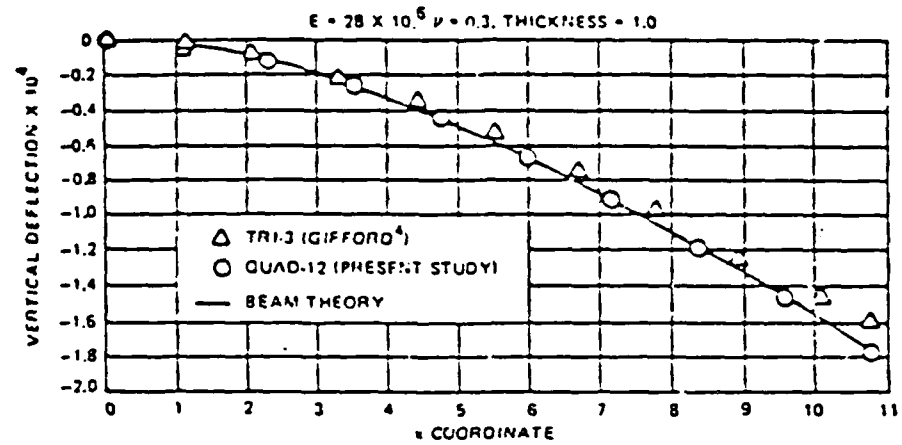
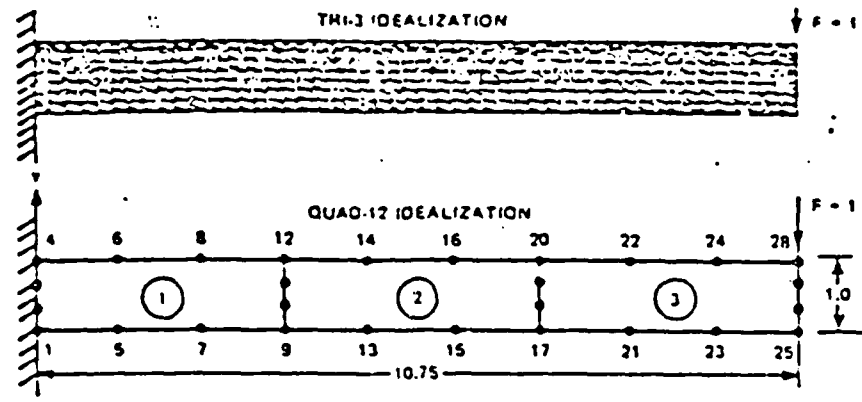


Figure 1. Graphical comparison of triangular and Quad-12 elements for a cantilever beam problem

II. PROBLEM FORMULATION

The first objective in the project was to develop a suitable finite element analysis program in order to study the local behavior of $\frac{dW}{dV}$ in cracked steel plates. PAST, a two-dimensional elastic-plastic finite element program, was selected as a starting software package. PAST, an acronym for *Plastic Axisymmetric and Planar Structures*, has been developed by the Navy over the last several years for the analysis of elastic-plastic crack problems [21-23].

The features of PAST are numerous. The program incorporates the 12-node quadrilateral isoparametric element adapted to plane stress, plane strain, and axisymmetric conditions of structural behavior. The displacements and geometry vary cubically in the Quad-12 element, thus allowing the accurate modeling of curved structural boundaries. By the nature of the Quad-12 element, relatively few elements are needed to effectively model most simple structures. PAST uses three basic elements in all: the standard Quad-12 element, the small circular *core* element which completely encloses a crack tip, and the enriched 12-node isoparametric element which has a corner node corresponding to a crack tip [22].

The outstanding feature of PAST is its non-linear stress and fracture mechanics analysis. It has the ability to treat cracks in fracture mechanics applications by two different methods, both of which will produce a direct calculation of the Mode I and Mode II stress intensity factors. Rice's *J-Integral* can be evaluated on up to ten different paths surrounding the crack tip. The *J-Integral* for elastic-plastic crack problems is given by Eq. 5.

PAST incorporates the incremental flow theory of plasticity and the Von Mises yield criterion with isotropic or kinematic hardening laws, or a combination of the two. The incremental plasticity theory is given as [23]:

$$\dot{\epsilon}_{ij} = \frac{1+\nu}{E} \dot{s}_{ij} + \frac{3}{2} f(\sigma_e) s'_{ij} \sigma'_e \quad (\text{for } \sigma'_e = \sigma_{yd, \text{current}} \text{ and } \sigma'_e > 0) \quad (13)$$

$$\dot{\epsilon}_{ij} = \frac{1+\nu}{E} \dot{s}_{ij} \quad (\text{otherwise}) \quad (14)$$

where:

$\dot{\epsilon}_{ij}$ = deviatoric strain rate components ($\dot{\epsilon}_{ij} = \dot{\epsilon}_{ij} - \frac{1}{3} \dot{\delta}_{pp} \delta_{ij}$)

s_{ij} = current deviatoric stress components ($s_{ij} = \sigma_{ij} - \frac{1}{3} \sigma_{pp} \delta_{ij}$)

s'_{ij} = deviatoric stress components measured from center of current yield surface ($s'_{ij} = s_{ij} - a_{ij}$)

a_{ij} = coordinates in stress space of center of yield surface

σ_e = von Mises effective stress = $\sqrt{\frac{3}{2} s_{ij} s_{ij}}$

$\sigma'_e = \sqrt{\frac{3}{2} s'_{ij} s'_{ij}}$

σ_{yd} = yield stress

In modeling the material in PAPST, an experimentally determined true stress-strain curve can be approximated using either a Ramberg-Osgood power-hardening model or a multilinear model. These models are graphically depicted in Fig. 2 [22]. The mathematical form of the power-hardening model is given as: [23]

$$\text{for } \sigma \leq \sigma_y, \quad \epsilon = \frac{\sigma}{E} \quad (15)$$

$$\text{for } \sigma > \sigma_y, \quad \epsilon = \frac{\sigma}{E} + \alpha \left[\frac{\sigma}{E} \left(\frac{\sigma}{\sigma_y} \right)^{n-1} - \frac{\sigma_y}{E} \right] \quad (16)$$

where n , α , and σ_y (the yield stress) are chosen to best model the observed behavior.

The mathematical form of the multilinear model is given as: [23]

$$\epsilon = \frac{\sigma}{E} + \frac{\alpha_1}{E} (\sigma_1 - \sigma_y) + \frac{\alpha_2}{E} (\sigma_2 - \sigma_1) + \cdots + \frac{\alpha_N}{E} (\sigma - \sigma_{N-1}) \quad (17)$$

where $\sigma_{N-1} < \sigma \leq \sigma_N$, σ_y is the yield stress, and

$$\alpha_N = \frac{E \Delta \epsilon_N - \Delta \sigma_N}{\Delta \sigma_N} \quad (18)$$

For this material model, the plastic strain rate is given by:

$$\dot{\epsilon}_{plastic} = \frac{\alpha_N \dot{\sigma}_e}{E} \quad \text{and} \quad f(\sigma_e) = \frac{\alpha_N}{E \sigma_e} \quad (19)$$

PAPST includes several other features: [21,23]

1. The crack tip elements include the plastic mode I singularity developed by Hutchinson, as opposed to the classical linear elastic singularity.
2. The Newton-Raphson iterative procedure is used to solve the non-linear equations under the restrictions of user-specified convergence criteria.
3. PAPST uses 4x4 numerical integration (Gaussian quadrature) to evaluate the conventional Quad-12 element's tangent stiffness matrices.
4. Loading, unloading, and reloading cycles can be used to simulate mechanically and/or thermally induced residual stresses and strains.
5. The first load increment is automatically calculated to correspond to the first yield in the specimen; the following load incrementation is user-specified.
6. Simulation of quasi-static crack growth.
7. A treatment of finite strain effects through the use of an updated Lagrangian formulation.
8. The capability to compute the applied tearing modulus T.
9. Large strain and large displacement formulation.

As an outgrowth of the non-linear stress analysis from PAPST, the strain energy $\frac{dW}{dV}$ was calculated from Eq. 7. It should be pointed out that this equation is only valid in the elastic region of the material. PAPST also has the capability to list those nodes that have undergone yielding. From this information, it can be determined where the formula for $\frac{dW}{dV}$ can and cannot be applied. To overcome

this restriction, $\frac{dW}{dV}$ can also be calculated from the area under the analytically generated true stress-strain diagram. This approach is valid for both the elastic and plastic regions. The non-linear stress analysis output from PAPST can be used to analytically draw the true stress-strain diagram; the area under this curve was computed and said to be equivalent to local $\frac{dW}{dV}$.

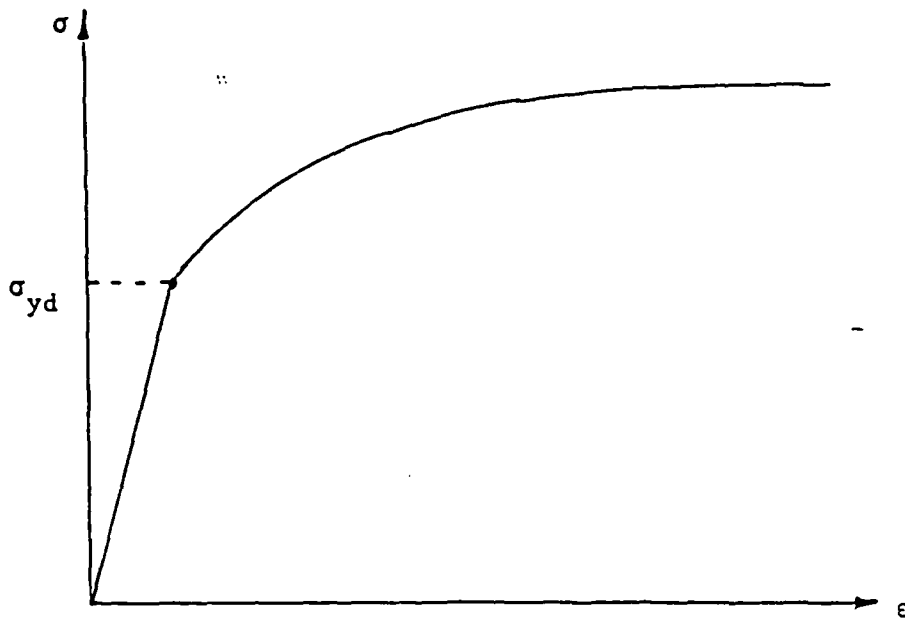


Figure 2a: Power Hardening Material Model

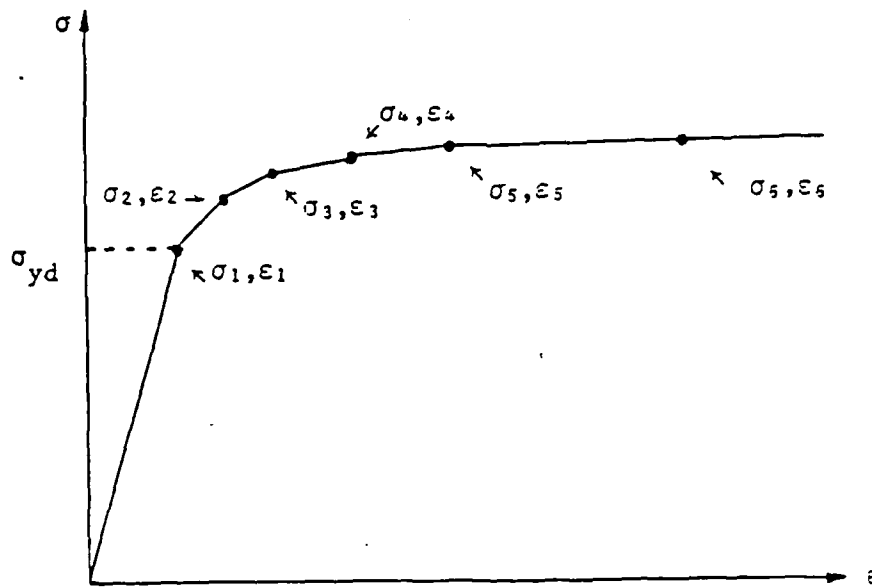


Figure 2b: Multilinear Material Model for $|N| = 6$

Figure 2. Graphical depiction of the material modeling available in PAPST

III. SOFTWARE DEVELOPMENT

A major portion of the research was devoted to the development of a suitable program to analyze the behavior of local $\frac{dW}{dV}$ in cracked steel plates. PAST, a two-dimensional elastic-plastic finite element program described extensively in section II, was selected as a starting software package. As PAST was used mainly for its non-linear stress analysis capabilities, several modifications and additions were made to the program to better serve the needs of the present research. The major addition was a subprogram which performed a complete energy solution and analysis. The modified version of the original program is henceforth referred to as *ARLPAST* in the rest of this manuscript.

There were three major areas in which PAST was modified:

1. Data preparation and pre-processing
2. Modifications to the running of the PAST stress analysis program
3. Several post-processors added which perform complete energy analyses including both analytical and graphical interpretation of output from the PAST stress analysis program

The data input for the main PAST program is quite extensive. It includes nodal connectivity and coordinates (both Cartesian and polar), a variety of loading options, graphical and data output options, angled and un-angled crack analysis, many fracture mechanics analysis options including calculation of the *J-Integral* on up to ten user-specified paths, and user-specified non-linear material modeling. To aid the user in entering this voluminous amount of data, an interactive pre-processor was added to the original package. This has significantly reduced the data preparation time.

The second major area of modification concerned the convergence criteria used

by PAPST in the non-linear stress analysis. The program's original convergence scheme was replaced by a more intelligent and versatile one. The new criteria reads in initial convergence parameters specified by the user in the data input. As the program runs through each load increment, these parameters are optimized for the most efficient convergence possible. In addition, these continuously variable convergence parameters are automatically tested to determine whether the resulting criteria is within acceptable limits.

The main program was also modified to read in raw data output options specified by the user, thereby printing out only selected parts of the output for *each increment*. These included:

- a. Strains and stresses for each element
- b. Normal strains at each node
- c. Normal stresses at each node
- d. Location and value of highest Von Mises stress
- e. Original (user and computer generated) nodal coordinates
- f. Nodal displacements

The third and most extensive area of modifications to the main PAPST program was the post-processing. This post-processing, now an integral part of ARL-PAPST, includes a complete analytical and graphical energy analysis of the specimen. The present capabilities include:

- a. Calculation of area under the true stress-strain diagram for any load increment and any user-specified node in the mesh. This provides a *direct* means of calculating local $\frac{dW}{dV}$, and is valid for nodes in both the elastic *and* plastic regions. A graph is produced of the true stress strain diagram in addition to a history of the incremental areas under the curve.
- b. Calculation of local $\frac{dW}{dV}$ using Eq. 7 for any node in the elastic region at any load increment.

- c. Plots of local $\frac{dW}{dV}$ (formula or direct) versus distance of corresponding node from crack tip.
- d. Plots of local $\frac{dW}{dV}$ (formula or direct) versus θ , the angle of the corresponding node from crack plane.
- e. Plots of the specimen idealization during loading, indicating the regions where yielding has taken place.

Thus, the original PAPST non-linear stress solver has been extensively modified and improved upon. The new package, ARLPAPST, is a much more versatile and capable program. Its advantages are summed as follows:

- a. More user-friendly.
- b. An extensive list of raw data output and graphical output options are now available.
- c. A more versatile and efficient convergence criterion for the non-linear stress analysis.
- d. A complete energy analysis of the specimen, including two methods to calculate local $\frac{dW}{dV}$ at a user-specified node and at a user-specified load increment.
- e. Several options available to graphically and analytically interpret the energy analysis.

IV. FINITE ELEMENT MODELING

The behavior of the local energy in the immediate vicinity of the crack tip was analyzed using ARLPAPST. All of the computer analysis was performed on a Digital VAX 11/782 super minicomputer. The original specimen analyzed is pictured in Fig. 3. As it is symmetric about the crack axis, only an idealized *upper symmetric half* of the specimen was modeled. The idealization shown uses the 12-node isoparametric quadrilateral elements discussed previously. Note how the elements are concentrated closer to the crack tip. A fine mesh is required for an accurate stress analysis close to the crack tip, as this is where the non-linear material behavior and plasticity is most evident. But as the distance from the crack tip increases, the density of the mesh can decrease. A detailed mesh far from the crack tip is both unnecessary and costly.

An experimental true stress-true strain diagram for A-517 steel was taken from the literature [14] and is shown in Fig. 4. This curve was modeled in a bi-linear fashion; the two points chosen from the curve are represented by:

$\sigma_1=107,400$ psi	$\epsilon_1=0.00358$	(yield)
$\sigma_2=108,570$ psi	$\epsilon_2=0.006$	(post-yield)

The other material properties used in the program were a Young's Modulus of 30 million psi and Poisson's ratio ν of 0.3. A load of 6000 lb. was used as a reference to which load increments were computed for data input in each of the computer runs.

Several different specimen geometries were analyzed, and are tabulated in table 2. For each of these geometries, several runs were made to vary the incremental loading of the specimen. When a new specimen geometry is first analyzed, a wide

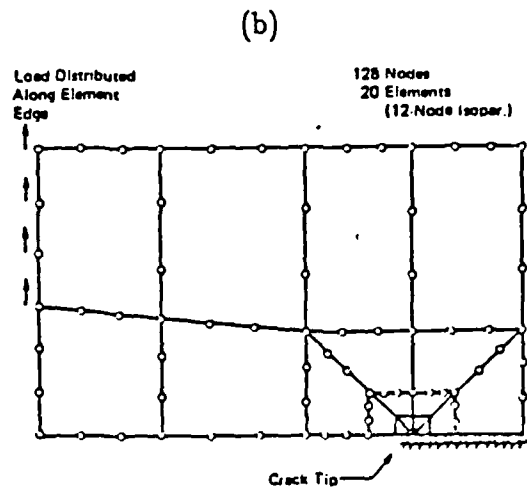
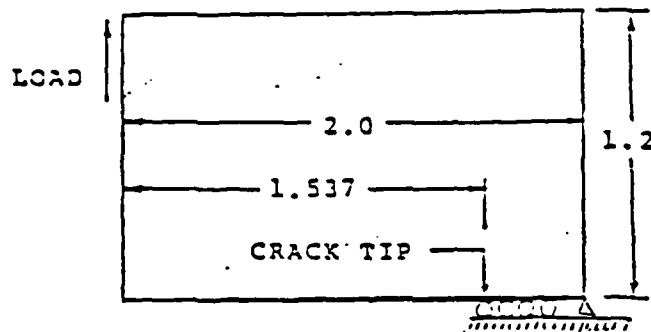
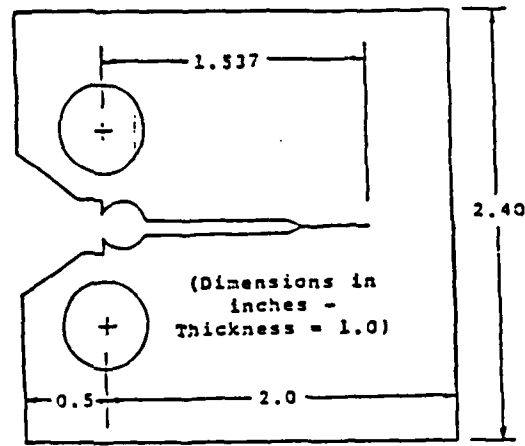


Figure 3. The original model analyzed, crack length = 1.537 inches
 a. Actual specimen geometry
 b. Idealized geometry (symmetric half)
 c. Structural idealization

range of load increments is usually chosen in order to gain a rough idea of how the specimen responds to the loading. In subsequent runs, the load increments are concentrated over a certain range to more closely study the fracture behavior of the specimen. The choice of load incrementation must be chosen in such a manner that the increments are close enough to permit efficient convergence and an accurate stress analysis. Yet there is a tradeoff, for as the number of increments is increased, so is the cost of the individual computer run. Analytical results are presented and discussed in the next section.

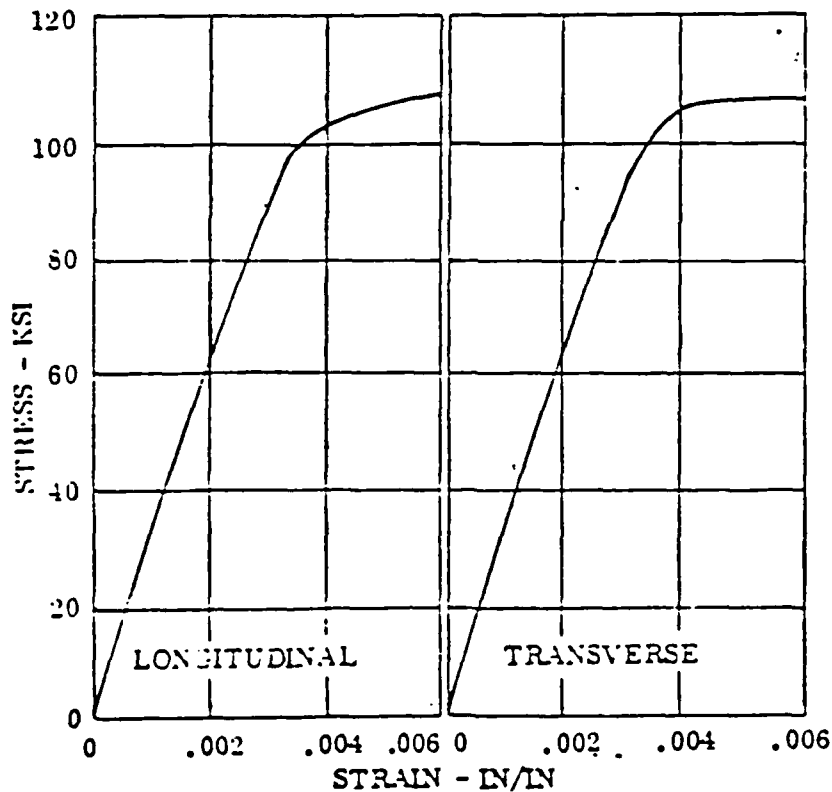


Figure 4. Experimental True Stress Strain curve for A-517 steel used for bi-linear modeling

Table 2. Compilation of different models analyzed in the present research

Run Number	Crack Length	Specimen Width	Number of Nodes	Number of Elements	Number of Increments	Maximum Load (lb.)
1	0.5	2.0	197	32	3	6600
2	0.5	2.0	197	32	4	60000
3	0.5	2.0	197	32	17	72000
4	0.5	2.0	197	32	19	126000
1	1.0	2.0	194	32	4	54000
2	1.0	2.0	194	32	20	63000
1	1.537	2.0	128	20	17	5820
1	1.537	2.0	243	40	7	5400
2	1.537	2.0	243	40	12	5840
3	1.537	2.0	243	40	16	5160
1	1.537	4.0	210	34	8	360000
2	1.537	4.0	210	34	9	222000
1	1.537	10.0	167	26	2	172200
1	1.643	2.0	243	40	21	3396
1	1.7685	2.0	243	40	21	5400
2	1.7685	2.0	243	40	24	1380

V. ANALYTICAL RESULTS AND DISCUSSION

The objective in our research has centered on studying the behavior of the local strain energy density $\frac{dW}{dV}$ in the vicinity of the crack tip. From the literature it is found that $\frac{dW}{dV}$ monotonically decays as the distance from the crack tip increases. From the non-linear stress analysis output from ARLPAPST, several energy analyses were performed in order to check this expected behavior.

A global analysis of the energy field around the crack tip is given in Fig. 5. This is a global analysis in the sense that the data represents practically all the nodes generated in the finite element mesh. In general, it can be seen that the energy steadily decreases with an increase in distance from the crack tip, as predicted in the literature. As Fig. 5 indicates, however, there are some energy values that do not follow this predicted behavior. This anomalous behavior of an increase in energy away from the crack tip was confirmed to be correct.

To study this anomalous behavior more closely, the analysis then narrowed to those nodes lying at a particular angle θ from the crack axis. As Fig. 6 shows, the curves at 30° and 50° exhibit the expected behavior of a decrease in energy with an increase in distance from the crack tip. However, the curve at $\theta = 0^\circ$, representing those nodes lying directly in front of the crack, exhibits a *minimum energy point* followed by an increase in energy. This unexpected behavior of an increase in energy with an increase in distance only occurs in those curves corresponding to $\theta = 0^\circ$, irrespective of the crack lengths and specimen dimensions.

From Fig. 3, it is seen that the crack axis is perpendicular to the direction of the loading. Secondly, a homogeneous material (A-517 steel) was used throughout the research. Thirdly, in all the specimens analyzed, plane strain conditions were maintained, thus eliminating the effects of plane stress. As a result, it is safe to

assume that the crack will propagate in a self-similar manner at $\theta = 0^\circ$. It was felt that there was a possible link between this anomalous behavior of $\frac{dW}{dV}$ in the $\theta = 0^\circ$ direction and the anticipated direction of crack growth at $\theta = 0^\circ$ which is coincidentally in the same direction.

The next step in the research was to study the effects of load in further detail on the variation of the local strain energy density. This is graphically depicted in Fig. 7. As the distance from the crack tip is increased, the energy initially decreases rather sharply. The curve then reaches a minimum point at roughly a radius of 0.22 inches from the crack tip. From this point to the right edge of the specimen (at 0.5 inches from the crack tip), an increase in energy occurs. At the lower loads, this increase is rather subtle. Yet, at the higher loads, the energy increases sharply and then appears to level off.

The minimum energy point that exists in each of the curves was referred to as $(\frac{dW}{dV})_{min}$ and occurs at a location r_{min} . As the load is increased on the specimen, this value of $(\frac{dW}{dV})_{min}$ becomes more sharply defined, i.e., the curve develops a more sharply defined cusp at the bottom. In addition, as the load is increased from 1200 lb. to 4800 lb., $(\frac{dW}{dV})_{min}$ increases. However, $(\frac{dW}{dV})_{min}$ for the curve at 5400 lb. is significantly lower, and it signifies that $(\frac{dW}{dV})_{min}$ attains a maximum value at a load between 4800 lb. and 5400 lb. Furthermore, at larger distances from the crack tip, it is seen that after an increase in energy, the curves tend to reach a constant energy value, a region in which the energy gradient is zero. This constant value of energy was referred to as $(\frac{dW}{dV})_{con}$; the region of constant energy starts occurring at a location r_{con} in front of the crack tip.

In order to determine the load at which $(\frac{dW}{dV})_{min}$ attains a maximum value, ARLPAPST was run with different load increments chosen so as to yield several energy values between the loads of 4800 lb. and 5400 lb. After plotting curves similar to those in Fig. 7, plots were produced of the minimum energy versus the

load. This is seen in Fig. 8. This figure shows more clearly how $(\frac{dW}{dV})_{min}$ steadily increases with an increase in load up to a maximum value around 4980 lb., and then sharply decreases with further increase in the load. The peak value of $(\frac{dW}{dV})_{min}$ was referred to as $(\frac{dW}{dV})_{min}^*$; the load at which $(\frac{dW}{dV})_{min}^*$ occurred was referred to as a *special critical load*, P_{crit} .

Our attention then turned to studying $(\frac{dW}{dV})_{con}$. From Fig. 7, it was seen that this parameter was near constant at some load. It was found that the value of $(\frac{dW}{dV})_{con}$ was almost constant, i.e., the energy gradient was closest to zero, at the critical load of 4980 lb. To isolate this behavior, Fig. 9 gives the energy curve at *this critical load* taken from a family of curves similar to those in Fig. 7. This curve clearly exhibits the very constant nature of energy far from the crack tip ($r > r_{con}$), and is designated by $(\frac{dW}{dV})_{con}^*$.

In order to assess the significance of $(\frac{dW}{dV})_{min}^*$ and $(\frac{dW}{dV})_{con}^*$, it was imperative to study the effects of different crack lengths on the behavior of the energy fields. The specimen geometry remained the same as mentioned in figure 3 (width=2 in., height=2.4 in., thickness=1 in.). In addition to the original crack length of 1.537 inches, specimens with crack lengths of 1.0, 1.643, and 1.7685 inches were analyzed. It was found that a global energy analysis of these specimens revealed the same anomalous behavior in energy in the direction $\theta = 0^\circ$ as discussed above.

Similar to the curve in Fig. 8, three different curves were drawn in Fig. 10 to further analyze the behavior of $(\frac{dW}{dV})_{min}$ versus load for specimens with different crack lengths. The first observation is that the peak energy value $(\frac{dW}{dV})_{min}^*$ for these curves are roughly the same and are approximately equal to $52 \text{ lb} - \text{in}/\text{in}^3$. Secondly, beyond the end of each curve, it was found that plastic collapse occurred in the specimen. It is safe to assume that the ends of these curves can be linearly extrapolated to cross over the load axis. At these points, $(\frac{dW}{dV})_{min} = 0$; this would correspond to a condition where all of the energy stored in the specimens has been

released and, as such, the condition corresponding to the failure of the specimens. Thus, the fracture load can be analytically predicted for specimens with different crack lengths. This fracture load can be directly compared with and verified by experimental data. Furthermore, from Fig. 10 it was found that for all three curves, the critical load corresponding to $(\frac{dW}{dV})_{min}^*$ is approximately 83% of the fracture load. Thus, $(\frac{dW}{dV})_{min}^*$ signifies a pre-failure condition which may be characteristic of the material.

As regards the criticality of $(\frac{dW}{dV})_{con}^*$, Fig. 11 and 12 represent the strain energy density versus radial distance from the crack tip for a wide range of external loads; the crack lengths used in these figures are 1.0 in. and 1.643 in., respectively. It can be seen from Fig. 11 and 12 that at a certain critical load which is dependent on the crack length, $(\frac{dW}{dV})_{con}^*$ remains constant over the distance $r \geq r_{crit}$. However, it should be noted that the values of $(\frac{dW}{dV})_{con}^*$ in Fig. 11 and 12 are the same and is equal to about $280 \text{ lb} - \text{in}/\text{in}^3$, as can be clearly seen in Fig. 13. Thus, $(\frac{dW}{dV})_{con}^*$ is independent of the crack length. It is also found that $(\frac{dW}{dV})_{con}^*$ is independent of the specimen dimensions, as can be clearly seen in Fig. 14. Recalling that both $(\frac{dW}{dV})_{min}^*$ and $(\frac{dW}{dV})_{con}^*$ are exhibited at a fixed percentage (83%) of the predicted fracture loads of various specimens having different crack length and geometry, it is observed that both these energy quantities refer to some "pre-fracture events" which are the characteristic of the material. It is assumed that $(\frac{dW}{dV})_{min}^*$ and $(\frac{dW}{dV})_{con}^*$ correspond to the local and global instability, respectively, prior to the final fracture of the specimens. (Note: the ratio of $(\frac{dW}{dV})_{con}^*$ to $(\frac{dW}{dV})_{min}^*$ is 5.4) The local instability can be further interpreted as signifying the crack initiation at $r = r_{min}^*$, requiring a relatively smaller level of energy. Likewise, the global instability can be further interpreted as signifying a much higher level of energy for possible slow crack growth, (up to $r = r_{crit}$) which is expected in the A-517 steel used in the present investigation.

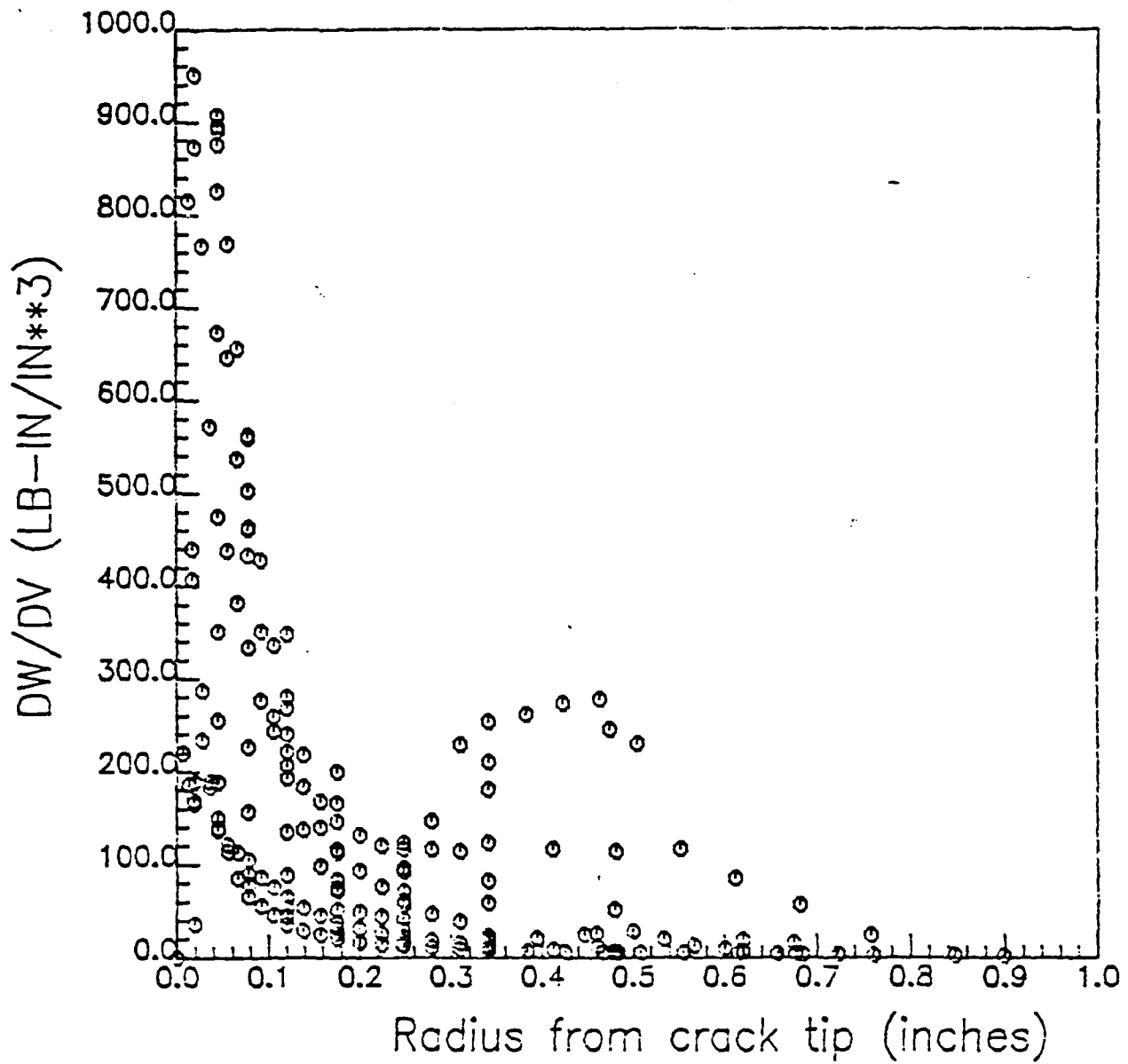


Figure 5. Global analysis of strain energy density versus radius (distance) from crack tip at a load of 4800 lb.

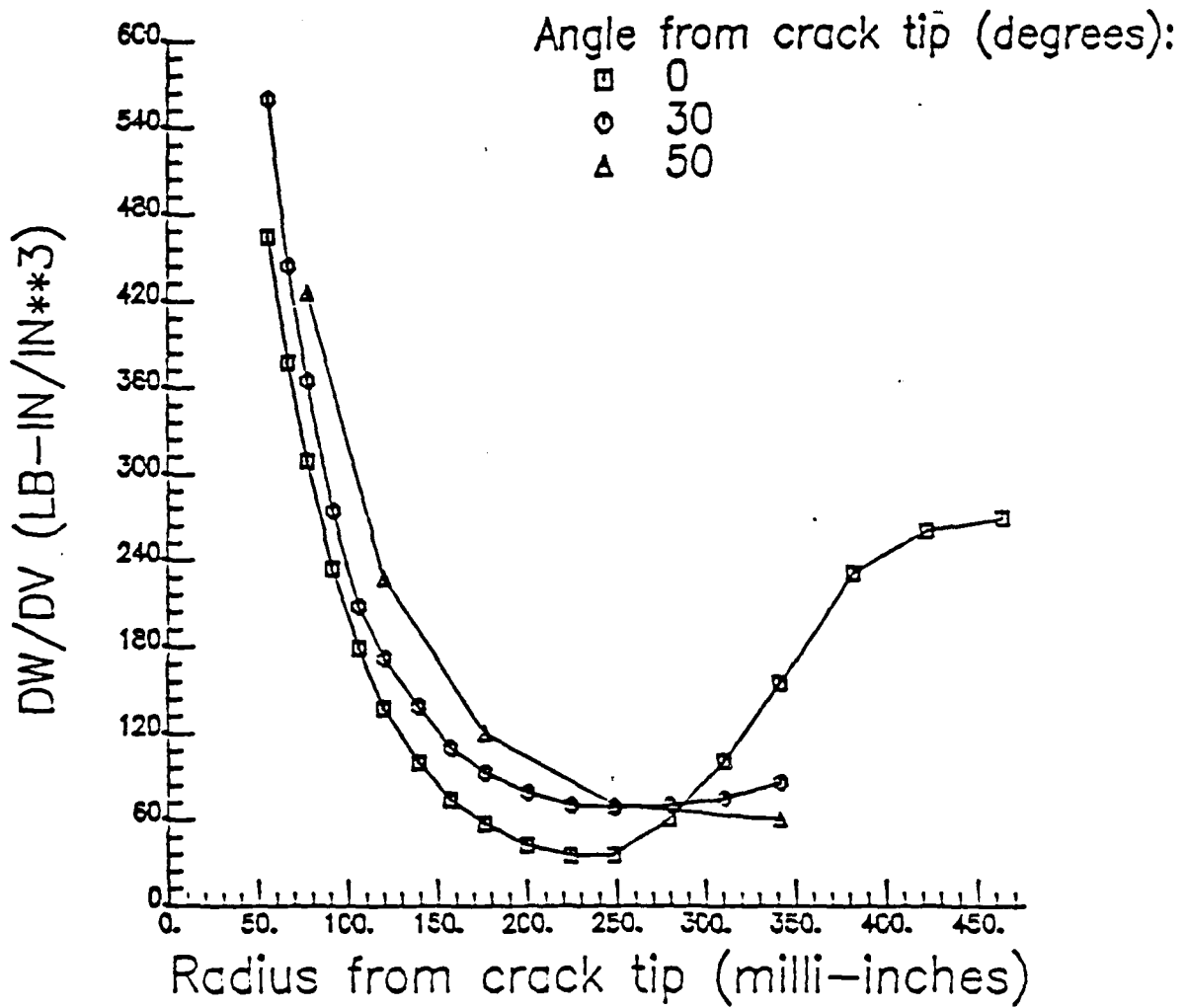


Figure 6. Comparison of strain energy density versus radius for nodes at 3 different angles from crack tip at a load of 4200 lb.

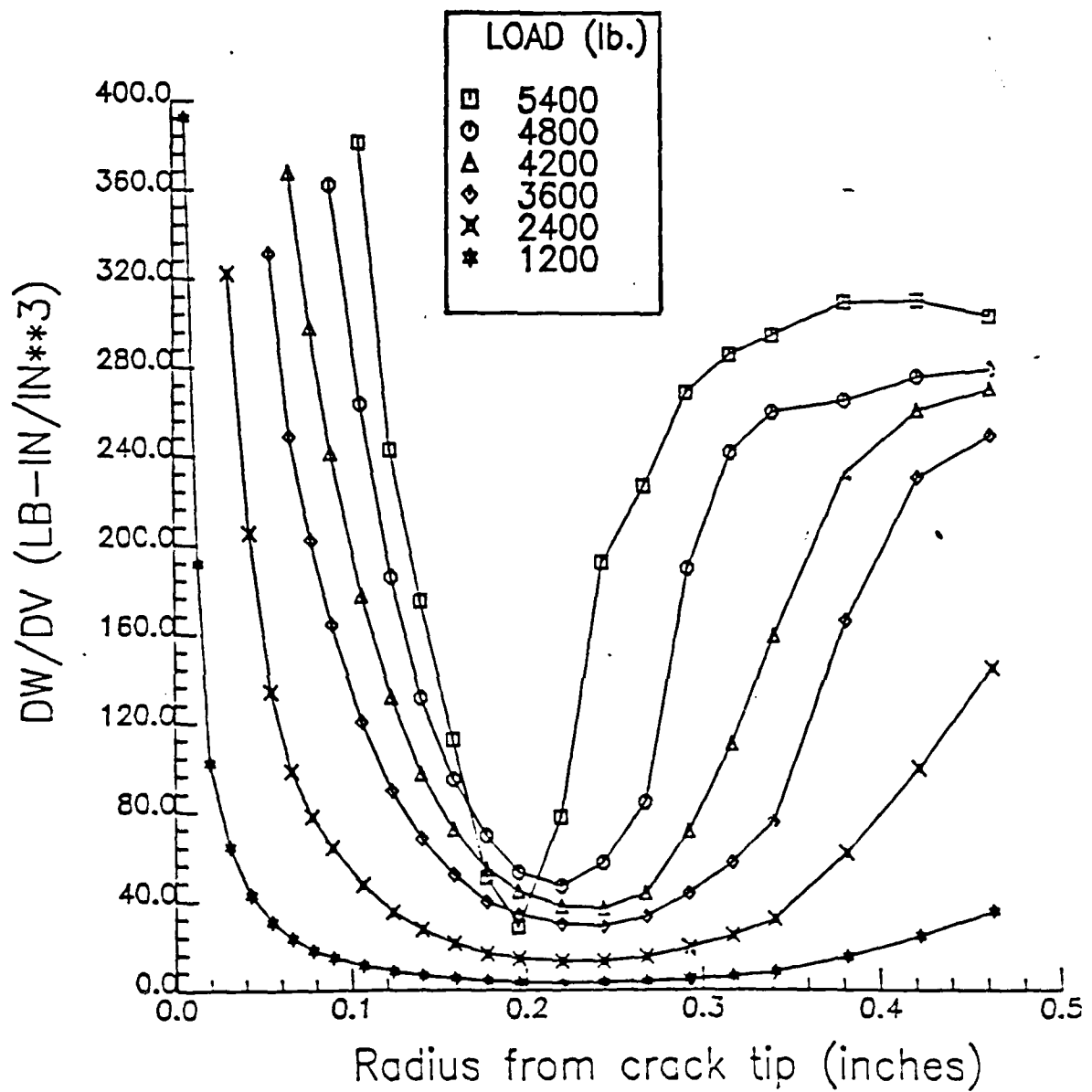


Figure 7. Comparison of strain energy density versus radius for different load increments at $\theta = 0^\circ$

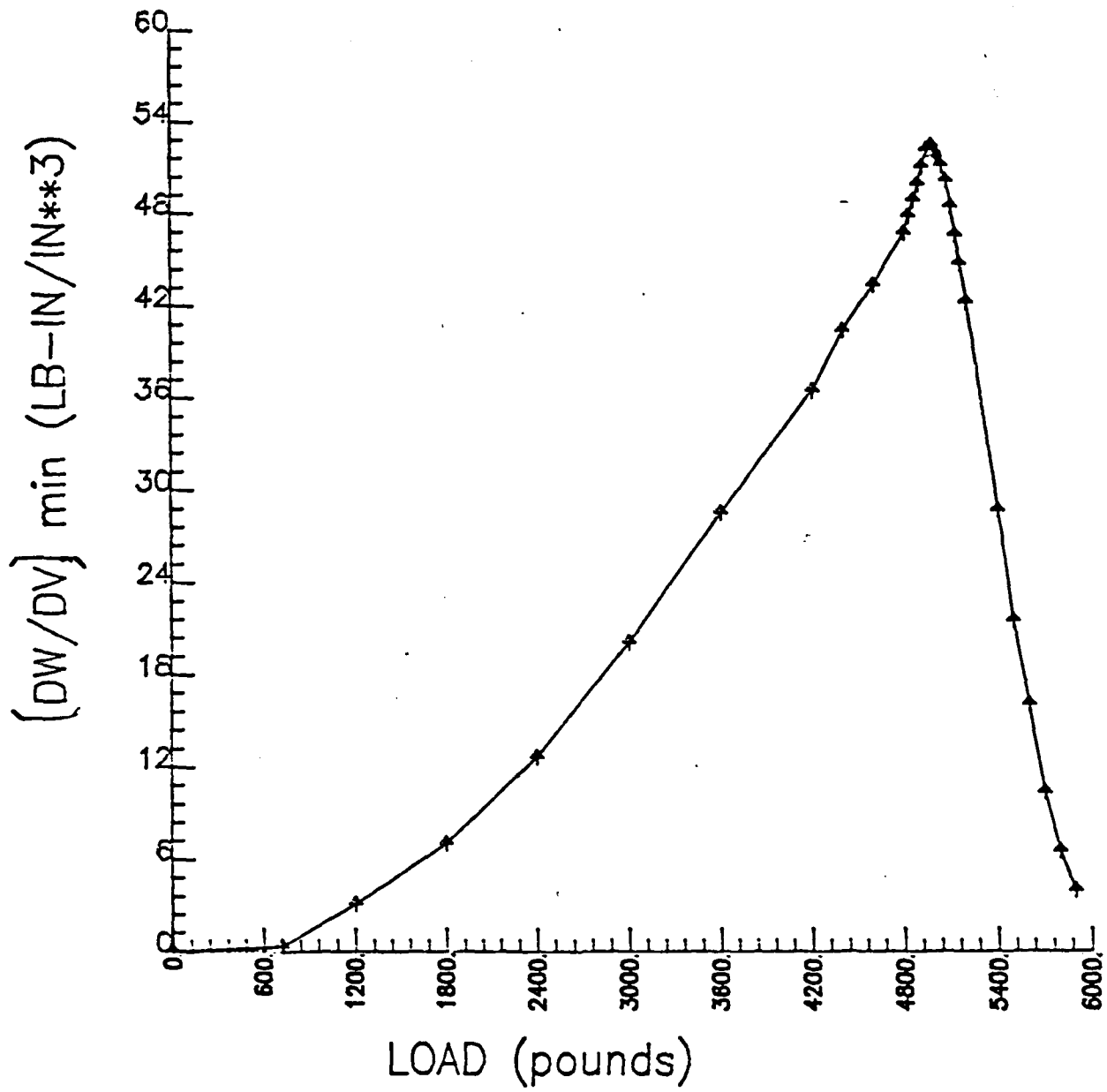


Figure 8. Analysis of minimum strain energy density versus load at which that minimum occurs for a crack length of 1.537 inches

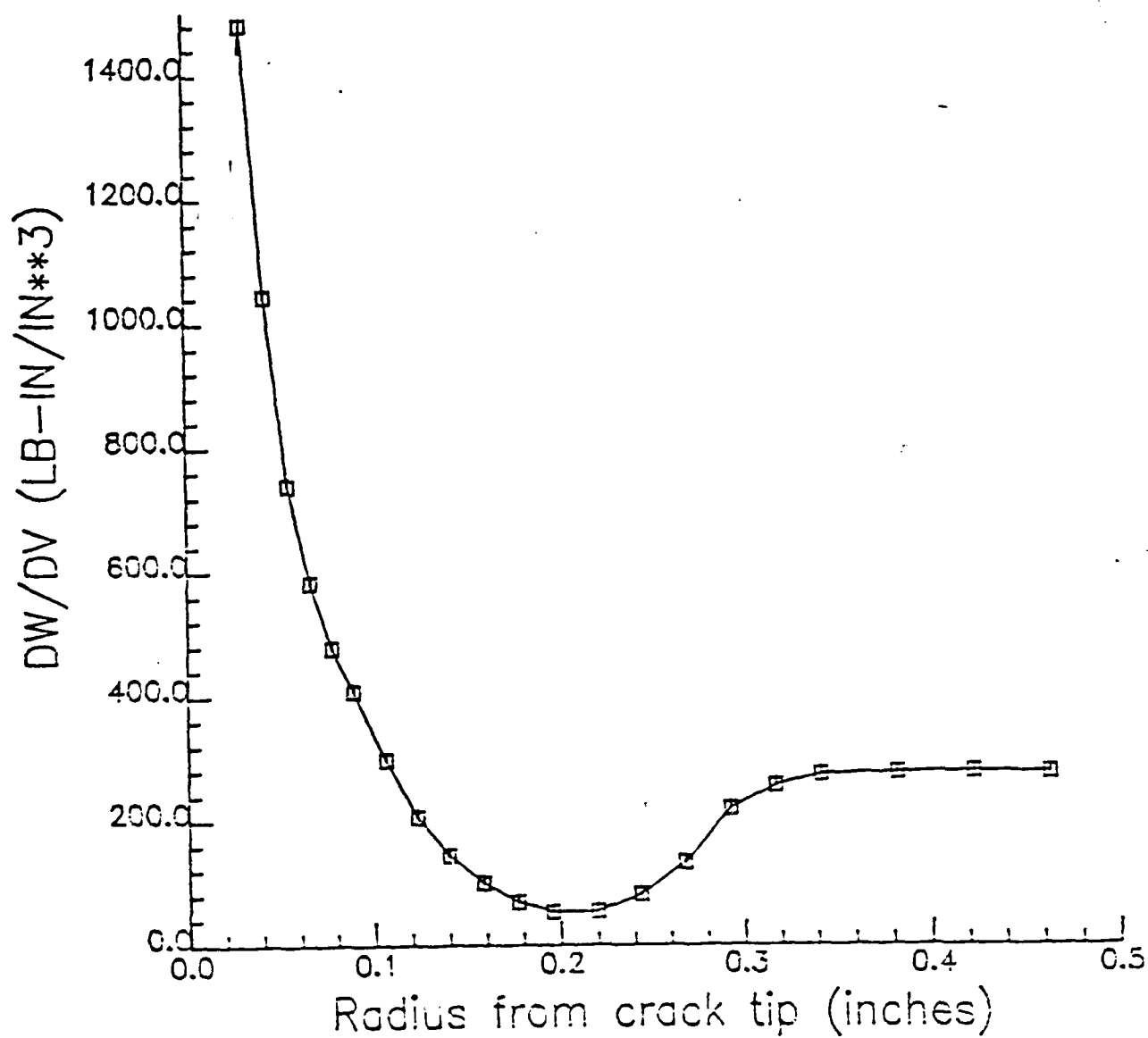


Figure 9. Shape of strain energy density versus radius curve at the critical load of 4980 lb.

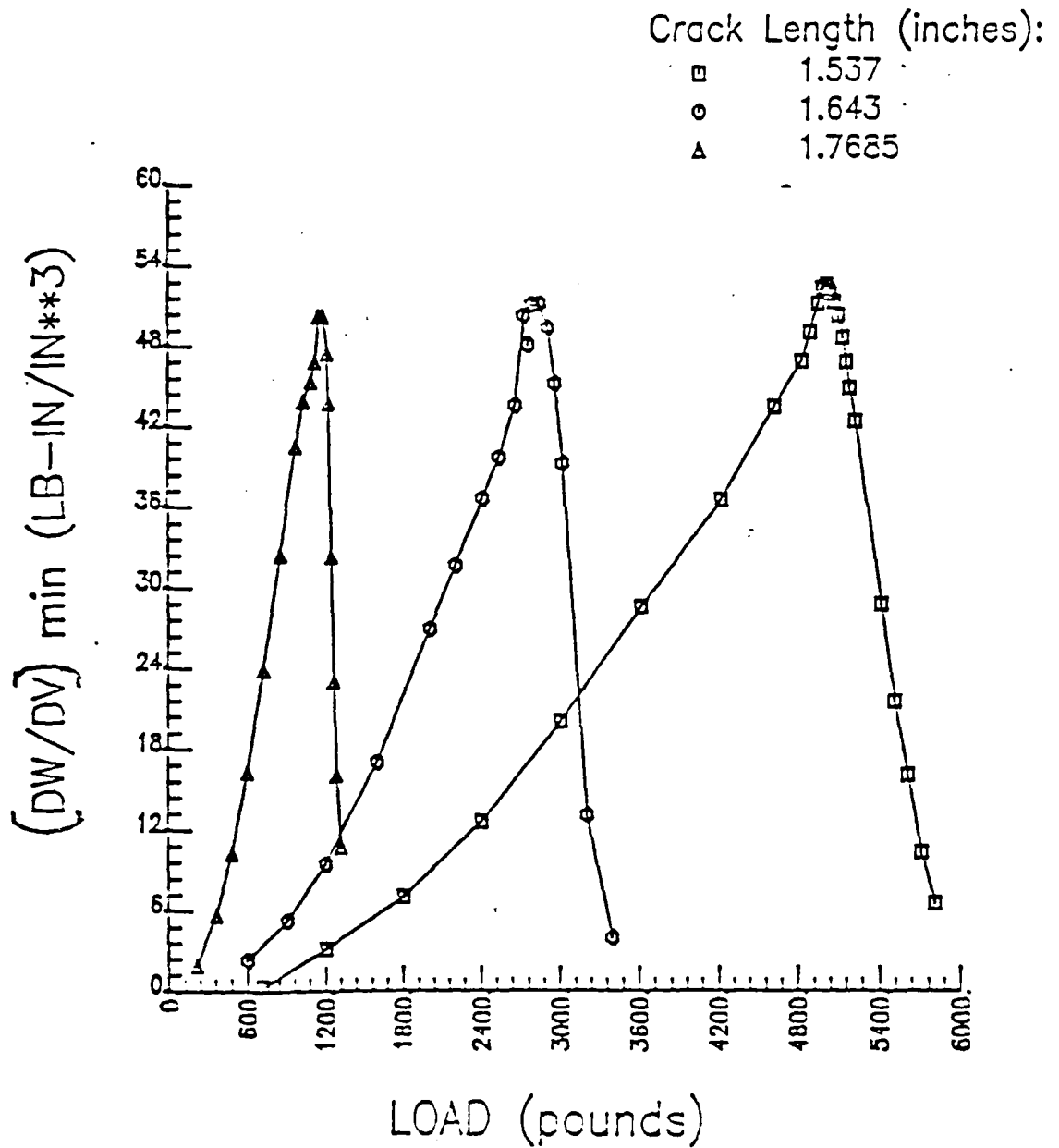


Figure 10. Effects of crack length on minimum strain energy density versus radius curves

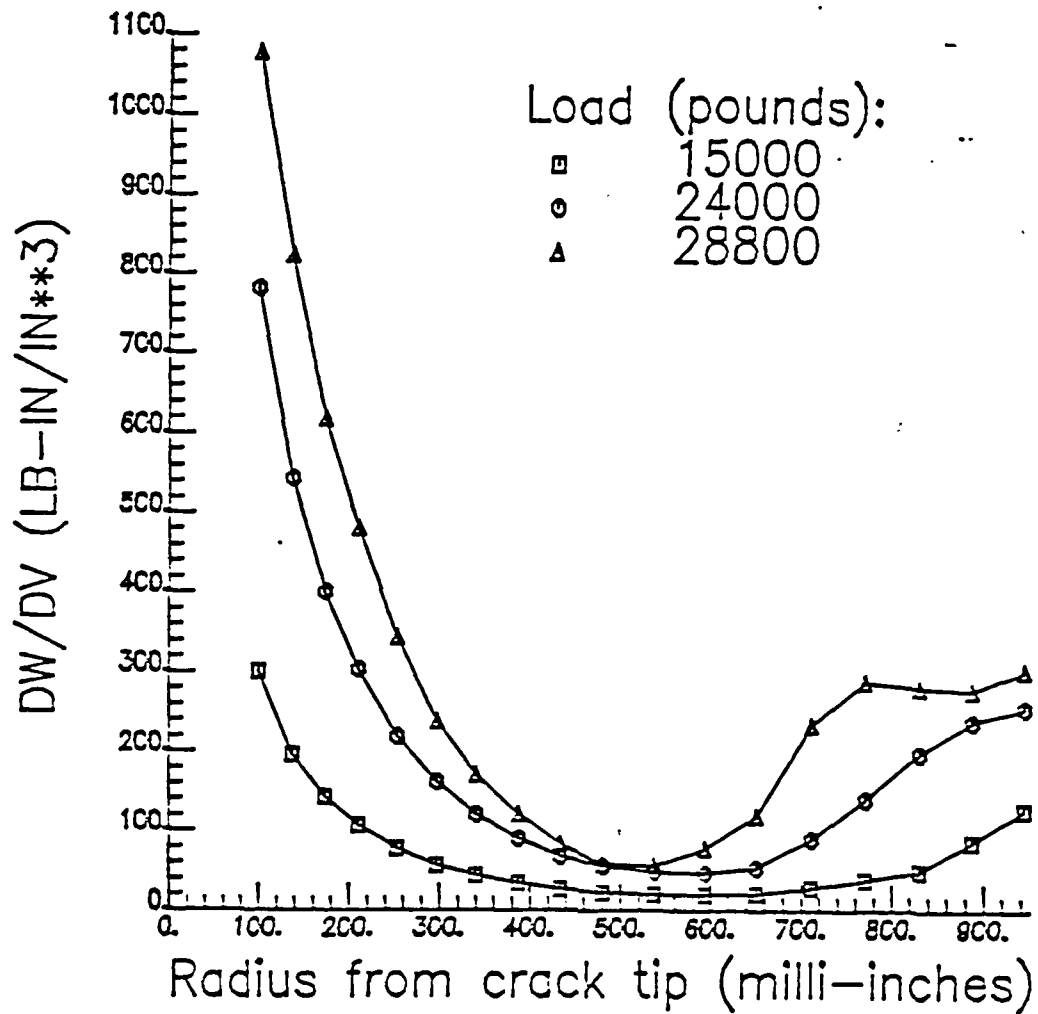


Figure 11. Strain energy density versus radius curves for specimen with crack length of 1.0 inches

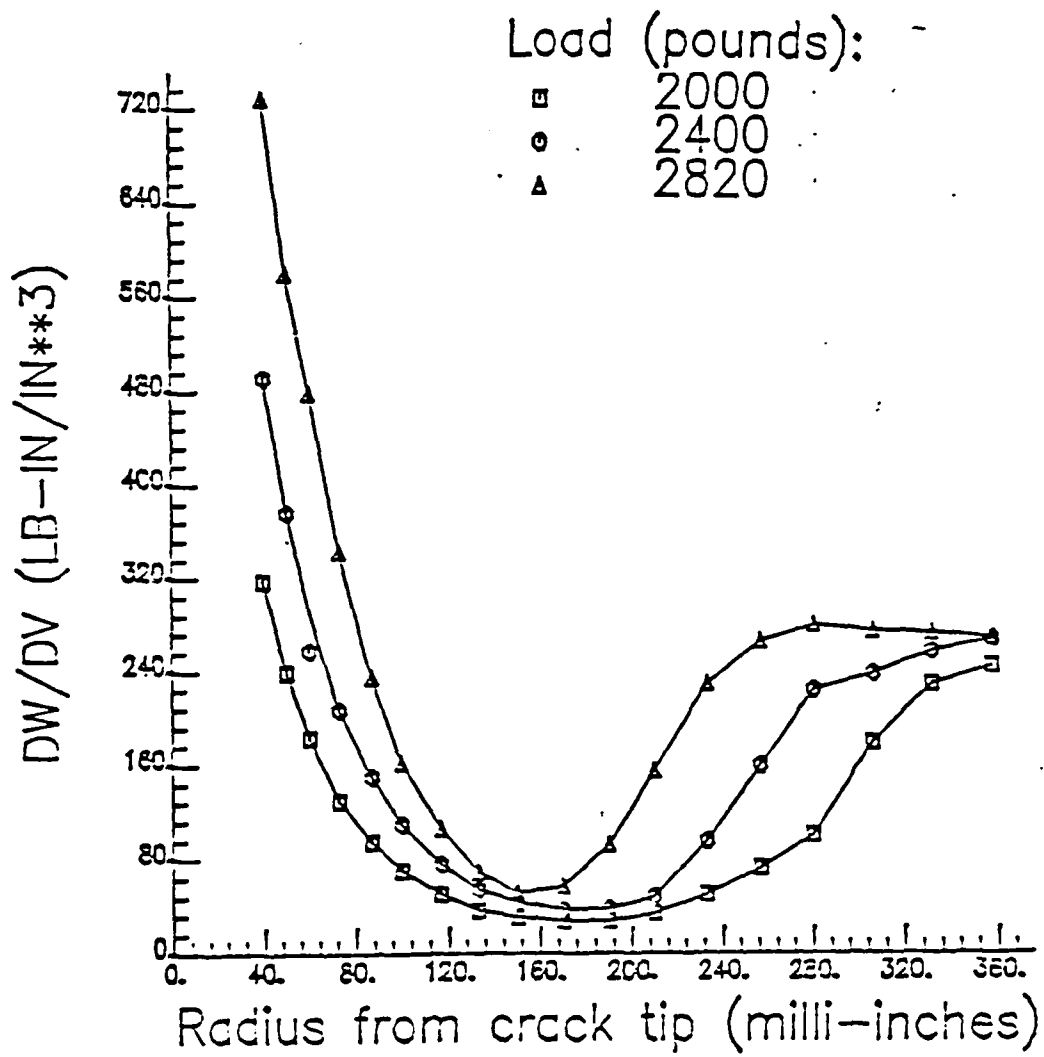


Figure 12. Strain energy density versus radius curves for specimen with crack length of 1.643 inches

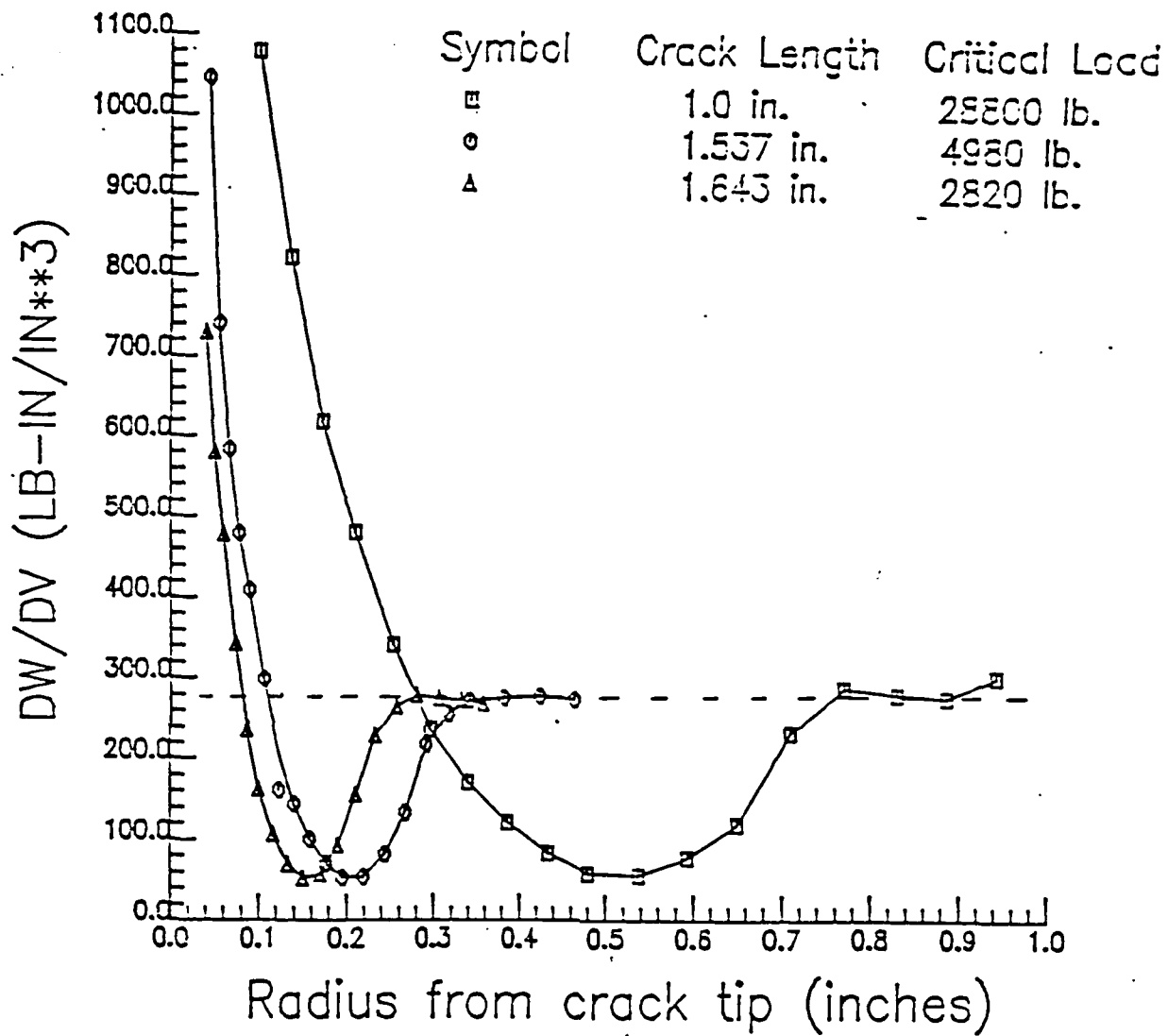


Figure 13. Effects of crack length on strain energy density versus radius curves

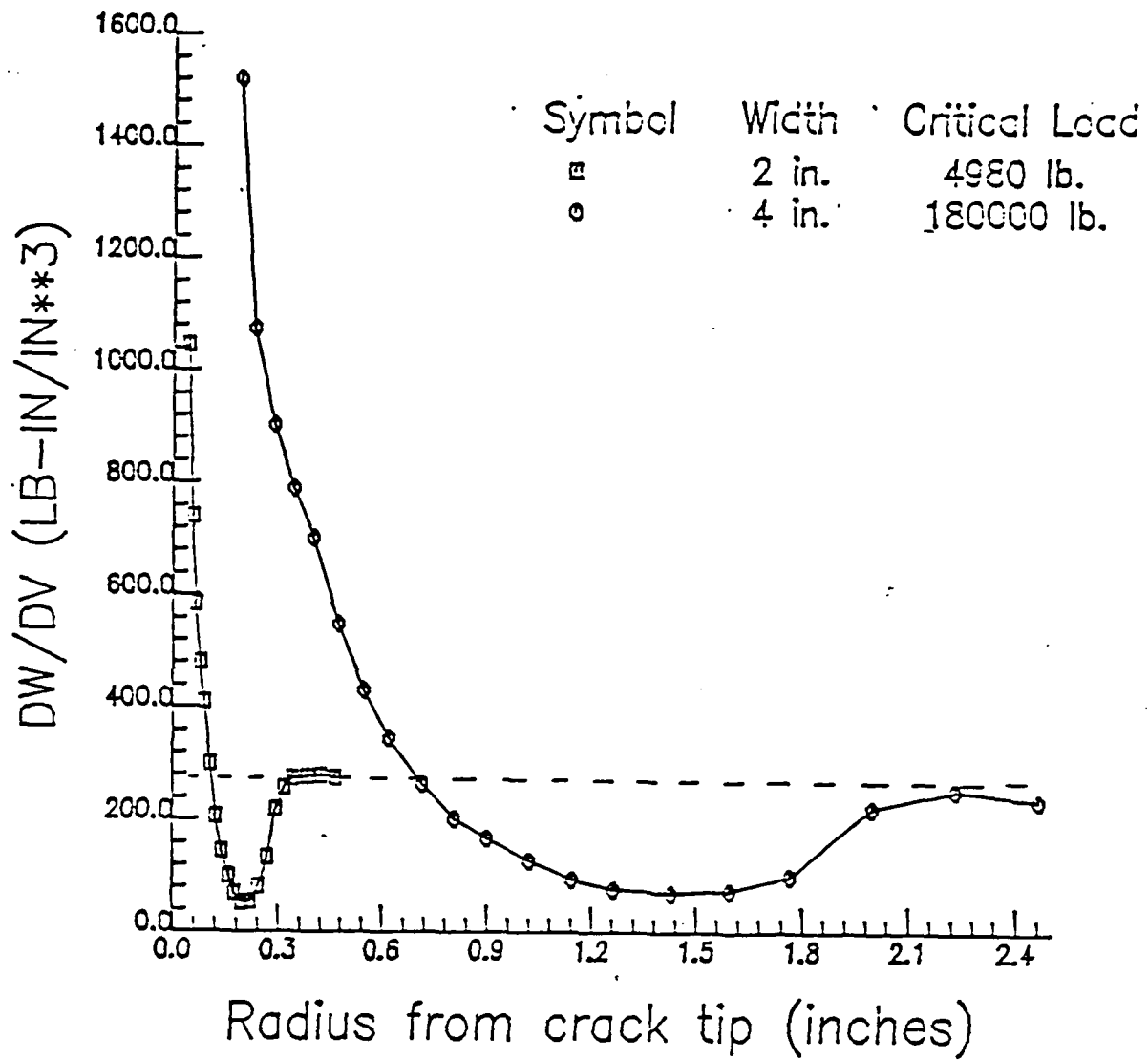


Figure 14. Effects of specimen width on strain energy density versus radius curves

VI. CONCLUSIONS

A computer program ARLPAPST has been developed to carry out two-dimensional non-linear finite element stress analysis in the neighborhood of a crack in A-517 steel compact tension specimens. A probable direction of crack propagation and loads corresponding to either catastrophic fracture or plastic collapse of specimens having different crack lengths have been predicted. In addition, two critical energy quantities, $(\frac{dW}{dV})_{min}^*$ and $(\frac{dW}{dV})_{con}^*$ have been established. These quantities are independent of the crack length and the specimen geometry, and always correspond to a fixed percentage (83%) of the predicted fracture loads for different specimens. For A-517 steel, $(\frac{dW}{dV})_{min}^*$ and $(\frac{dW}{dV})_{con}^*$ are $52 \text{ lb} - \text{in}/\text{in}^3$ and $280 \text{ lb} - \text{in}/\text{in}^3$, respectively. It is observed that $(\frac{dW}{dV})_{min}^*$ signifies a local instability leading to crack initiation at a fixed distance ahead of the crack; and $(\frac{dW}{dV})_{con}^*$ signifies a global instability just before the slow crack growth, followed by the final failure of the specimen.

VIII. REFERENCES

1. Broek, David "Elementary Engineering Fracture Mechanics" Martinus Nijhoff Publishers: Boston, 1982.
2. Griffith, A.A. "The Phenomenon of Rupture and Flow in Solids", *Philosophical Transactions of the Royal Society of London*, A 221 (1921) pp. 163-197.
3. Liebowitz, H., ed. "Fracture: An Advanced Treatise", Vol. 1, Academic Press: New York, 1968.
4. Suh, Nam P., and Arthur P.L. Turner "Elements of the Mechanical Behavior of Solids" McGraw-Hill Book Company: New York, 1975.
5. Irwin, G.R., *Fracture of Metals*, American Society of Metals, Cleveland, Ohio, 1948.
6. Orowan, E., "Energy Criterion of Fracture, Welding Criterion of Fracture", *Welding Research Supplement*, p. 157, 1955.
7. Sih, G.C., and Luciano deOliveira Faria, eds. "Fracture Mechanics Methodology: Evaluation of Structural Components Integrity" Martinus Nijhoff Publishers: The Hague, 1984.
8. Wells, A.A., "Unstable Crack Propagation in Metals: Cleavage and Fast Fracture", *Proc. of the Crack Propagation Symposium*, Cranfield, p. 210, 1961.
9. Rice, J.R., "A Path Independent Integral and the Approximate Analysis of Strain Concentration by Notches and Cracks", *Journal of Applied Mechanics*, 35, p. 379, 1968.
10. Liu, H.W. "On the Fundamental Basis of Fracture Mechanics", *Engineering Fracture Mechanics*, Vol. 17, No. 5, 1983, pp. 425-438.
11. Sih, George C., ed. "Methods of Analysis and Solutions of Crack Problems", *Mechanics of Fracture*, Vol. I, Noordhoff International Publishing: Leyden, 1972.
12. Sih, G.C. and E. Madenci "Fracture Initiation under Gross Yielding: Strain Energy Density Criterion" *Engineering Fracture Mechanics*, Vol. 18, No. 3, pp. 667-677, 1983.
13. Higdon, Archie and Edward H. Ohlsen, et al. "Mechanics of Materials" John Wiley & Sons: New York, 1978.
14. Hucek, Harold J., ed. "Structural Alloys Handbook, Vol. I", Battelle's Columbus Laboratories: Columbus, Ohio, 1981

15. *Engineering Properties of Steel*, American Society of Metals, Metals Park, Ohio, 1982.
16. Cook, Robert D. "Concepts and Applications of Finite Element Analysis" John Wiley & Sons: New York, 1974.
17. Gallagher, Richard H. "Finite Element Analysis: Fundamentals" Prentice-Hall, Inc.: Englewood Cliffs, New Jersey, 1975.
18. Hinton, E., and Owen, D.R.J. "An Introduction to Finite Element Computations" Pineridge Press Limited: Swansea, U.K., 1979.
19. Hinton, E., and Owen, D.R.J. "Finite Element Programming" Academic Press: London, 1977.
20. Norrie, D.H., and deVries, G. "An Introduction to Finite Element Analysis" Academic Press: New York, 1978.
21. Gifford, L. Nash, and Peter D. Hilton "Preliminary Documentation of PAPST: Non-linear Fracture Stress Analysis by Finite Elements" DTNSRDC, 1981.
22. Gifford, L. Nash "APFS: Second Generation Two-dimensional Fracture Mechanics and Stress Analysis by Finite Elements" DTNSRDC, 1978.
23. Hilton, P.D. and L.N.Gifford "Elastic-Plastic Finite-Element Analysis for Two-Dimensional Crack Problems" *Elastic-Plastic Fracture: Second Symposium, Volume I - Inelastic Crack Analysis*, ASTM STP 809, C.F. Shih and J.P. Gudas, eds., American Society for Testing and Materials, 1983, pp. I256-I273.

END

10-86

DTIC